 CMES, vol.6, no.2, pp.169-188, 2004

Meshless Local Petrov-Galerkin (MLPG) approaches for solving 3D Problems in elasto-statics

Z. D. Han[1] **and S. N. Atluri**[1]

Abstract: Three different truly Meshless Local Petrov-Galerkin (MLPG) methods are developed for solving 3D elasto-static problems. Using the general MLPG concept, these methods are derived through the local weak forms of the equilibrium equations, by using different test functions, namely, the Heaviside function, the Dirac delta function, and the fundamental solutions. The one with the use of the fundamental solutions is based on the local unsymmetric weak form (LUSWF), which is equivalent to the local boundary integral equations (LBIE) of the elasto-statics. Simple formulations are derived for the LBIEs in which only weakly-singular integrals are included for a simple numerical implementation. A novel definition of the local 3D sub-domain is presented, which enables the numerical integrations to be performed in an accurate and efficient way, based on a truly meshless implementation. The augmented radial basis functions (RBF) and the moving least squares (MLS) are chosen to construct the shape functions, for the three MLPG methods. Numerical examples are included to demonstrate that the present methods are very promising for solving the elastic problems, as compared to the traditional Galerkin Finite Element Method.

keyword: Meshless Local Petrov-Galerkin approach (MLPG), Local Boundary Integral Equations (LBIE), Radial Basis Functions (RBF), Moving Least Squares (MLS).

1 Introduction

The Galerkin Finite Element Method has found extensive engineering acceptance as well as a commercial market. Compared with its convenience and flexibility in use, the finite element method (FEM) has been plagued for a long time, by the inherent problems such as locking, poor derivative solutions, etc. It is well known that the accuracy of the FEM relies on the quality of the mesh and the element type. First, a good-quality of the mesh cannot be always achieved, especially when adaptive refinement and adaptive re-meshing are required for 3D problems. It has also been found that only simple quadrilateral or hexahedral elements have achieved considerable success for explicit dynamic analysis. However, the use of such elements is limited by the mesh generation.

In contrast, the truly meshless local Petrov-Galerkin (MLPG) approach has become very attractive as a very promising method for solving 3D problems. The MLPG concept was presented in Atluri and Zhu (1998). The main advantage of this method, over the widely used finite element methods, is that it does not need any mesh, either for the interpolation of the solution variables or for the integration of the weak forms. It has been developed as a general framework for solving partial differential equations by Atluri and colleagues. Under this framework, the PDEs can be solved in their various ***local*** symmetric or unsymmetric weak forms, by using a variety of interpolation methods (trial functions), test functions, integration schemes with/without background cells, and their flexible combinations. The MLPG domain methods have been studied in [Atluri and Zhu (1998), Atluri and Shen (2002a,b)]. Recently, the MLPG method has been applied to boundary integral equations, as MLPG/BIE [Atluri, Han and Shen (2003), Han and Atluri (2003b)]. The many research successes in solving PDEs, and demonstrates that the MLPG method, and its variants, become some of the most promising alternative methods for computational mechanics. Unfortunately, most research is restricted in solving 2D problems. It is more challenging to apply the MLPG for solving 3D problems, because of the difficulty in handling the local integrals over the intersection of the local test-function domain and the global boundary of the arbitrary 3D solution domain. The representative 3D works include the papers of [Li, Shen, Han and Atluri (2003)]

[1] Center for Aerospace Research & Education
University of California, Irvine
5251 California Avenue, Suite 140
Irvine, CA, 92612, USA

for 3D elastic problems by using MLPG domain methods, and [Han and Atluri(2003b)] for 3D elastic fracture problem by using MLPG BIE methods. A summary of the literature on MLPG, to date, appears in the monograph by Atluri(2004).

In the present work, three MLPG methods are developed for solving 3D elasto-static problems. The first method employs a local symmetric weak form (LSWF), and the shape functions are also chosen as the test functions, which leads to a symmetric system of equations. The similar work has been done for solving 2D elastic problems by Atluri, Kim and Cho (1999), in which the MLS approximation was used. Although the MLS approximations have some drawbacks in dealing with the essential boundary conditions, they can be straightforwardly applied to 3D cases, by using the numerical techniques developed for 2D problems [Atluri, Kim and Cho (1999)]. One of the major advantages of the MLS is that, the shape functions are constructed from the local points only, with the high order continuities. In the present study, the augmented RBF approximations are also used to construct shape functions [Golberg, Chen and Bowman (1999)]. They have some distinct advantages over the MLS approximation including that, the shape functions possess the delta function property, and the second derivatives of the shape functions are smoother, and are computationally less costly. Its delta function property makes it possible to directly enforce the essential boundary conditions through the collocation method. *However, it should be pointed out that the RBF approximations give non-continuous shape functions, if they are used in local meshless way*. It is not possible, using the RBF approximation, to construct shape functions in the global way for 3D problems, which leads to a fully-populated system matrix. In addition, the compactly-supported RBFs are also required to avoid the round-off errors, when a large number of nodes are included in the solution domain, especially for 3D cases.

The second MLPG method in the present study is the same as the first one, except that the Heaviside function is used as the test function [Atluri and Shen (2002a,b)]. The advantage of this method is the lesser cost in assembling the system equations.

The third MLPG method employs a local unsymmetric weak form and uses the static fundamental solution as the test function. This method is equivalent to the local boundary integral equation (LBIE) method. Although only a boundary discretization is necessary for linear boundary value problems, the global boundary element methods entails fully populated coefficient matrices, which hinders their application to large-scale problems with complex geometry. Besides, in the BEM, the evaluation of the unknown function and/or its gradients at any single point within the domain of the problem involves the calculation of an integral over the entire global boundary, which is tedious and inefficient in the global boundary element method. In the LBIE, however, all the field values within the domain of the problem are interpolated through the shape functions and the matrices are banded. The LBIE has been applied for 2D potential problems [Zhu, Zhang, and Atluri (1998)], and 2D elasto-static problems [Atluri, Sladek, Sladek and Zhu (2000)]. Recently, it has also been successfully applied in the 2D Laplace-transform domain [Sladek, Sladek and Zhang (2003)] and the 2D frequency domain [Sellountos and Polyzos (2003)]. All these studies were carried out for 2D problems, in which the special numerical quadrature schemes were introduced to evaluate the strongly singular integrals. In the present study, we use the simple non-hyper-singular BIE formulations, given in the paper of Han and Atluri (2003a) with the combination of the augmented RBF approximation. With these formulations, the strong singularities in the LBIE can be also avoided by using the rigid body motion idea, as in the conventional global BIEs. It makes the present LBIE methods to be more numerically efficient. In addition, the formulations presented by Han and Atluri (2003a) are also numerically tractable when the traction BIEs are applied in the local domain for contact and fracture problems [Han and Atluri (2004)].

In the general MLPG approach, the local test domains can be arbitrary, such as spheres, cubes, and ellipsoids in 3D. However, the local sub-domains become very complicated, for the points which are located on, or near, the global boundaries, because of the intersection between the simple sub-domain and the boundary surfaces. It hinders the MLPG to be truly meshless for realistic 3D solution domains. In the present study, a method is developed to define the local sub-domains as spheres, with the use of polyhedrons to subdivide the local spherical surfaces for all surface integrals, in a piece-wise fashion. The polyhedrons can be also so chosen to match the global boundary of the complicated 3D solution domain.

The following discussion begins with the brief descrip-

tion of the augmented RBF and MLS approximations in Section 2. The various MLPG methods in different weak forms are presented in Section 3. Section 4 deals with the numerical aspects of treating the local domains. A method is presented to define the local 3D sub-domains in Section 5. Numerical examples for 3D elasticity problems are given in Section 6. Then paper ends with conclusions and discussions in Section 7.

2 Interpolation Approximation

2.1 The RBF approximation

For a so-called meshless implementation, a meshless interpolation scheme is required, in order to approximate the trial functions over the solution domain. The interpolation schemes with the radial basis functions (RBF) are becoming attractive in meshless methods, because of the delta function property of the shape functions and the simplicity of their derivatives. The polynomials are also introduced to overcome their lack of completeness [Golberg, Chen and Bowman (1999)].

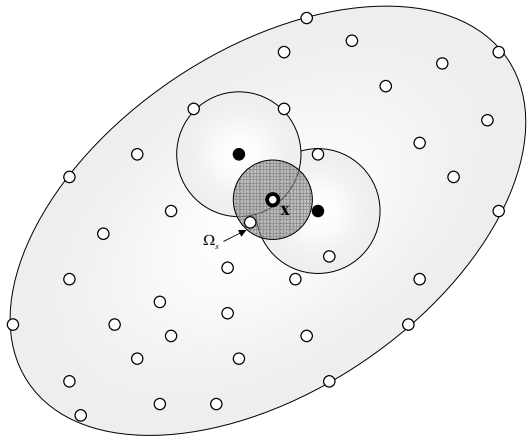

Figure 1 : a local sub-domain around point **x**

Consider a sub-domain Ω_s, the neighborhood of a point **x**, which is local in the solution domain, shown in Figure 1. To approximate the distribution of function u in Ω_s, over a number of scattered points $\{\mathbf{x}_i\}$, $(i = 1,2,...,n)$, the local augmented RBFs interpolate $u(\mathbf{x})$ of u, $\forall \mathbf{x} \in \Omega_s$, can be defined by

$$u(\mathbf{x}) = \mathbf{R}^T(\mathbf{x})\mathbf{a} + \mathbf{P}^T(\mathbf{x})\mathbf{b} \quad \forall \mathbf{x} \in \Omega_s \tag{1}$$

where $\mathbf{R}^T(\mathbf{x}) = [R_1(\mathbf{x}), R_2(\mathbf{x}), ..., R_n(\mathbf{x})]$ is a set of radial basis functions centered around the n scattered points; $\mathbf{a}^T = [a_1, a_2, ..., a_n]$ is a constant vector containing the coefficients; $\mathbf{P}^T(\mathbf{x}) = [p_1(\mathbf{x}), p_2(\mathbf{x}), ..., p_m(\mathbf{x})] = [1, x, y, z, x^2, y^2, z^2, xy, yz, zx, ...]$ is a monomial basis of order m; $\mathbf{b}^T = [b_1, b_2, ..., b_m]$ is a constant vector containing the coefficients. The radial basis function has the following general form

$$R_i(\mathbf{x}) = R_i(r_i) \quad \text{and} \quad r_i = \|\mathbf{x} - \mathbf{x}_i\| \tag{2}$$

To determine the coefficients **a** and **b**, one may enforce the interpolation to satisfy the given values at the scattered points as:

$$u(\mathbf{x}_i) = \mathbf{R}^T(\mathbf{x}_i)\mathbf{a} + \mathbf{P}^T(\mathbf{x}_i)\mathbf{b} \quad i = 1,2,...,n \quad \text{or}$$
$$\mathbf{u}^e = \mathbf{R}_0\mathbf{a} + \mathbf{P}_0\mathbf{b} \tag{3a}$$

and

$$\sum_{i=1}^{n} p_j(\mathbf{x}_i)a_i = 0 \quad j = 1,2,...,m \quad \text{or} \quad \mathbf{P}_0^T\mathbf{a} = \mathbf{0} \tag{3b}$$

One may write Eq. (3) in the matrix form as:

$$\begin{bmatrix} \mathbf{R}_0 & \mathbf{P}_0 \\ \mathbf{P}_0^T & \mathbf{0} \end{bmatrix} \begin{Bmatrix} \mathbf{a} \\ \mathbf{b} \end{Bmatrix} = \begin{Bmatrix} \mathbf{u}^e \\ \mathbf{0} \end{Bmatrix} \tag{4}$$

By solving Eq. (4), the constant vectors can be obtained as:

$$\begin{Bmatrix} \mathbf{a} \\ \mathbf{b} \end{Bmatrix} = \begin{bmatrix} \mathbf{R}_0 & \mathbf{P}_0 \\ \mathbf{P}_0^T & \mathbf{0} \end{bmatrix}^{-1} \begin{Bmatrix} \mathbf{u}^e \\ \mathbf{0} \end{Bmatrix} \equiv \mathbf{G} \begin{Bmatrix} \mathbf{u}^e \\ \mathbf{0} \end{Bmatrix} \tag{5}$$

By substituting the solution of Eq. (5) into Eq. (1), the interpolation can be expressed as:

$$u(\mathbf{x}) = \left[\mathbf{R}^T(\mathbf{x}), \mathbf{P}^T(\mathbf{x})\right] \mathbf{G}\mathbf{u}^e \equiv \mathbf{\Phi}^T(\mathbf{x})\mathbf{u}^e \quad \forall \mathbf{x} \in \Omega_s \tag{6}$$

where by definition, $\mathbf{\Phi}(\mathbf{x})$ are the shape functions as:

$$\mathbf{\Phi}^T(\mathbf{x}) = \left[\mathbf{R}^T(\mathbf{x}), \mathbf{P}^T(\mathbf{x})\right] \mathbf{G} \tag{7}$$

The derivatives of the shape functions, $\mathbf{\Phi}_{,j}(\mathbf{x})$, can be obtained as:

$$\mathbf{\Phi}^T_{,j}(\mathbf{x}) = \left[\mathbf{R}^T_{,j}(\mathbf{x}), \mathbf{P}^T_{,j}(\mathbf{x})\right] \mathbf{G} = \left[\frac{d\mathbf{R}^T(\mathbf{x})}{dr} r_{,j}, \mathbf{P}^T_{,j}(\mathbf{x})\right] \mathbf{G} \tag{8}$$

Although there are wide choices for the RBFs, practical applications have focused on a limited number of functions to obtain the unique solution of Eq. (4), including thin plate splines (TPS), multiquadrics (MQ), Gaussians. *It should be pointed out that the shape functions are non-continuous if only some local points are involved in Eq. (1).* If all nodes are used, the matrix $\mathbf{G}$ in Eq. (5) are fully populated, which is not efficient and accurate, when a 3D model contains a large number of nodes. In the present study, the compactly supported RBFs are used in a local way, as:

$$R_i(r) = \begin{cases} (1-\frac{r}{r_{i0}})^3(3\frac{r}{r_{i0}}+1) & r \le r_{i0} \\ 0 & r > r_0 \end{cases} \tag{9}$$

where r_{i0} is the radius of the support size of node i.

2.2 The moving least squares (MLS)

The MLS method of interpolation is generally considered to be one of the best schemes to interpolate random data with a reasonable accuracy [Atluri and Zhu (1998)]. Although the nodal shape functions that arise from the MLS approximation have a very complex nature, they always preserve completeness up to the order of the chosen basis, and robustly interpolate the irregularly distributed nodal information. The MLS scheme has been widely used in domain discretization methods. With the MLS, the distribution of function u in Ω_s can be approximated as,

$$u(\mathbf{x}) = \mathbf{p}^T(\mathbf{x})\mathbf{a}(\mathbf{x}) \quad \forall \mathbf{x} \in \Omega_s \tag{10}$$

where $\mathbf{p}^T(\mathbf{x}) = [p_1(\mathbf{x}), p_2(\mathbf{x}), ..., p_m(\mathbf{x})]$ is a monomial basis of order m; and $\mathbf{a}(\mathbf{x})$ is a vector containing coefficients, which are functions of the global Cartesian coordinates $[x_1, x_2, x_3]$, depending on the monomial basis. They are determined by minimizing a weighted discrete L_2 norm, defined, as:

$$\begin{aligned} J(\mathbf{x}) &= \sum_{i=1}^{m} w_i(\mathbf{x})[\mathbf{p}^T(\mathbf{x}_i)\mathbf{a}(\mathbf{x}) - \hat{u}_i]^2 \\ &\equiv [\mathbf{P}\cdot\mathbf{a}(\mathbf{x}) - \hat{\mathbf{u}}]^T \mathbf{W} [\mathbf{P}\cdot\mathbf{a}(\mathbf{x}) - \hat{\mathbf{u}}] \end{aligned} \tag{11}$$

where $w_i(\mathbf{x})$ are the weight functions and $\hat{u}_i$are the fictitious nodal values.

The stationarity of J in Eq. (11), with respect to $\mathbf{a}(\mathbf{x})$ leads to following linear relation between $\mathbf{a}(\mathbf{x})$ and $\hat{\mathbf{u}}$,

$$\mathbf{A}(\mathbf{x})\mathbf{a}(\mathbf{x}) = \mathbf{B}(\mathbf{x})\hat{\mathbf{u}} \tag{12}$$

where matrices $\mathbf{A}(\mathbf{x})$ and $\mathbf{B}(\mathbf{x})$ are defined by

$$\mathbf{A}(\mathbf{x}) = \mathbf{P}^T\mathbf{W}\mathbf{P} \quad \mathbf{B}(\mathbf{x}) = \mathbf{P}^T\mathbf{W} \quad \forall \mathbf{x} \in \partial\Omega_x \tag{13}$$

Once coefficients $\mathbf{a}(\mathbf{x})$ in Eq. (12) are determined, one may obtain the approximation from the nodal values at the local scattered points, by substituting them into Eq. (10), as

$$u(\mathbf{x}) = \mathbf{\Phi}^T(\mathbf{x})\hat{\mathbf{u}} \quad \forall \mathbf{x} \in \partial\Omega_x \tag{14}$$

where $\mathbf{\Phi}(\mathbf{x})$ is the so-called shape function of the MLS approximation, defined as,

$$\mathbf{\Phi}(\mathbf{x}) = \mathbf{p}^T(\mathbf{x})\mathbf{A}^{-1}(\mathbf{x})\mathbf{B}(\mathbf{x}) \tag{15}$$

The weight function in Eq. (11) defines the range of influence of node I. Normally it has a compact support. The derivatives of the shape functions in Eq. (15) can obtained by differentiate them respect to x_i [Atluri and Zhu (1998)]. The continuity of the shape functions is controlled , by that of the weight functions[Atluri and Shen, 2000a & 2000b].

3 MLPG domain methods

3.1 Local symmetric weak-forms (LSWF) of elasticity

Consider a linear elastic body in a 3D domain Ω, with a boundary $\partial\Omega$. The solid is assumed to undergo infinitesimal deformations. The equations of balance of linear and angular momentum can be written as:

$$\sigma_{ij,j} + f_i = 0; \quad \sigma_{ij} = \sigma_{ji}; \quad ()_{,i} \equiv \frac{\partial}{\partial \xi_i} \tag{16}$$

where σ_{ij} is the stress tensor, which corresponds to the displacement field u_i; f_i is the body force. The corresponding boundary conditions are given as follows,

$$u_i = \overline{u}_i \quad \text{on} \quad \Gamma_u \tag{17a}$$

$$t_i \equiv \sigma_{ij} n_j = \overline{t}_i \quad \text{on} \quad \Gamma_t \tag{17b}$$

where $\overline{u}_i$ and $\overline{t}_i$ are the prescribed displacements and tractions, respectively, on the displacement boundary Γ_u and on the traction boundary Γ_t, and n_i is the unit outward normal to the boundary Γ.

The strain-displacement relations are:

$$\varepsilon_{kl} = \frac{1}{2}(u_{k,l} + u_{l,k}) \tag{18}$$

The constitutive relations of an isotropic linear elastic homogeneous solid are:

$$\sigma_{ij} = E_{ijkl}\varepsilon_{kl} = E_{ijkl}u_{k,l} \tag{19}$$

where

$$E_{ijkl} = \lambda\delta_{ij}\delta_{kl} + \mu(\delta_{ik}\delta_{jl} + \delta_{il}\delta_{jk}) \tag{20}$$

with λ and μ being the Lame's constants.

In the local Petrov-Galerkin approaches, one may write a weak form over a local sub-domain Ω_s, which may have an arbitrary shape, and contain the a point $\mathbf{x}$ in question. A generalized local weak form of the differential equation (16) over a local sub-domain Ω_s, can be written as:

$$\int_{\Omega_s} (\sigma_{ij,j} + f_i) v_i d\Omega = 0 \tag{21}$$

where u_i and v_i are the trial and test functions, respectively.

By applying the divergence theorem, Eq. (21) may be rewritten in a symmetric weak form as:

$$\int_{\partial\Omega_s} \sigma_{ij} n_j v_i d\Gamma - \int_{\Omega_s} (\sigma_{ij} v_{i,j} - f_i v_i) d\Omega = 0 \tag{22}$$

Imposing the boundary conditions in (17), one obtains

$$\int_{L_s} t_i v_i d\Gamma + \int_{\Gamma_{su}} t_i v_i d\Gamma + \int_{\Gamma_{st}} \overline{t}_i v_i d\Gamma - \int_{\Omega_s} (\sigma_{ij} v_{i,j} - f_i v_i) d\Omega = 0 \tag{23}$$

where Γ_{su} is a part of the boundary $\partial\Omega_s$ of Ω_s, over which the essential boundary conditions are specified. In general, $\partial\Omega_s = \Gamma_s \cup L_s$, with Γ_s being a part of the local boundary located on the global boundary, and L_s being the other part of the local boundary which is inside the solution domain. $\Gamma_{su} = \Gamma_s \cap \Gamma_u$ is the intersection between the local boundary $\partial\Omega_s$ and the global displacement boundary Γ_u; $\Gamma_{st} = \Gamma_s \cap \Gamma_t$ is a part of the boundary over which the natural boundary conditions are specified.

Therefore, a local symmetric weak form (LSWF) in linear elasticity can be written as:

$$\int_{\Omega_s} \sigma_{ij} v_{i,j} d\Omega - \int_{L_s} t_i v_i d\Gamma - \int_{\Gamma_{su}} t_i v_i d\Gamma = \int_{\Gamma_{st}} \overline{t}_i v_i d\Gamma + \int_{\Omega_s} f_i v_i d\Omega \tag{24}$$

It should be pointed out that the essential boundary conditions can not be imposed directly even with the use of the RBF approximation, because the shape function possesses the delta property only at the corresponding node. Although one may impose the essential boundary conditions at all nodes on the prescribed displacement boundary, these conditions are still not satisfied for all points on the boundary except the nodal points. The reason is that the values at these points through the RBF approximation depend not only on the boundary nodes, but also the related ones inside the domain. This is quite different from those in the element-based methods, in which the boundary values are interpolated through only the nodes at the boundary nodes. The details for enforcing the essential boundary conditions have been reported by Zhu and Atluri (1998), and Atluri and Shen (2002a).

3.2 Local unsymmetric weak-forms (LUSWF) of elasticity

Let v_i be the trial functions, the weak form of Eq. (16) can also be written, without the boundary condition, as:

$$\int_{\Omega_s} (\sigma_{ij,j} + f_i) v_i d\Omega = 0 \tag{25}$$

Applying the divergence theorem two times in Eq. (25), we obtain:

$$\int_{\Gamma_s} t_j v_j \, dS - \int_{\Gamma_s} u_m (n_n E_{ijmn} v_{j,i}) \, dS + \int_{\Omega_s} u_m (E_{ijmn} v_{j,i})_{,n} d\Omega + \int_{\Omega_s} f_i v_i \, d\Omega = 0 \tag{26}$$

Consider a point unit load applied in an arbitrary direction $\mathbf{e}^p$ at a generic location $\mathbf{x}$ in a linear elastic isotropic homogeneous infinite. It is well-known that the displacement and stress solution corresponding to this unit point load are given as (Kelvin's solution):

$$u_i^{*p}(\mathbf{x},\xi) = \frac{1}{16\pi\mu(1-\upsilon)r}[(3-4\upsilon)\delta_{ip} + r_{,i}r_{,p}] \tag{27a}$$

$$\sigma_{ij}^{*p}(\mathbf{x},\xi) = \frac{1}{8\pi(1-\upsilon)r^2} [(1-2\upsilon)(\delta_{ij}r_{,p} - \delta_{ip}r_{,j} - \delta_{jp}r_{,i}) - 3r_{,i}r_{,j}r_{,p}] \tag{27b}$$

This fundamental solution has some basic properties, including

$$\int_{\Omega_s} \sigma_{ij,j}^{*p}(\mathbf{x},\xi) dS + \delta_{pi} = 0 \quad \text{for} \quad \forall \mathbf{x} \in \Omega \tag{28}$$

By taking the fundamental solution $u_i^{*p}(\mathbf{x},\xi)$ as the test functions $v_i(\xi)$, and with the consideration of its properties in Eq. (28), we re-write Eq. (26) in the form as the local boundary integral equations (LBIE):

$$u_p(\mathbf{x}) = \int_{\Gamma_s} t_i(\xi) u_i^{*p}(\mathbf{x},\xi) \, dS - \int_{\Gamma_s} u_i(\xi) t_i^{*p}(\mathbf{x},\xi) \, dS + \int_{\Omega_s} f_i(\xi) u_i^{*p}(\mathbf{x},\xi) \, d\Omega \tag{29}$$

Further more, Eq. (29) can also be simplified with the basic properties of the fundamental solutions as [Han and Atluri (2003a)]:

$$\int_{\Gamma_s} t_i(\xi) u_i^{*p}(\mathbf{x},\xi) \, dS - \int_{\Gamma_s} [u_i(\xi) - u_i(\mathbf{x})] t_i^{*p}(\mathbf{x},\xi) \, dS + \int_{\Omega_s} f_i(\xi) u_i^{*p}(\mathbf{x},\xi) \, d\Omega = 0 \tag{30}$$

which is equivalent to the rigid body motion idea used in the global BEM.

It should be pointed out that, Eq. (30) is based on the displacement BIEs, and holds the same form when point $\mathbf{x}$ approaches to the global boundary, Γ. In addition, the local unsymmetric weak form can be also used for the traction BIEs, which is more suitable for the crack and contact problems. One may write a **vector** weak form of Eq. (16) by taking the gradients of the fundamental solution as the test function [as originally proposed in Okada, Rajiyah, and Atluri (1988,1989), and extended in Han and Atluri (2003a)]. One may obtain the traction LBIE formulation as:

$$-t_b(\mathbf{x}) = \int_{\Gamma_s} t_q(\xi) n_a(\mathbf{x}) \sigma_{ab}^{*q}(\mathbf{x},\xi) \, dS + \int_{\Gamma_s} D_p u_q(\xi) n_a(\mathbf{x}) \Sigma_{abpq}^{*}(\mathbf{x},\xi) \, dS + \int_{\Omega_s} f_q(\xi) n_a(\mathbf{x}) \sigma_{ab}^{*q}(\mathbf{x},\xi) \, d\Omega \tag{31}$$

in which Σ_{abpq}^{*} is the derived kernel function defined as:

$$\Sigma_{ijpq}^{*}(\mathbf{x},\xi) = E_{ijkl} e_{nlp} \sigma_{nq}^{*k}(\mathbf{x},\xi) \tag{32}$$

Eq. (31) is the non-hypersingular integral equations. It can be simply regularized by applying the basic properties of the fundamental solution in Eq. (28), as:

$$0 = \int_{\Gamma_s} [t_q(\xi) - n_p(\xi)\sigma_{pq}(\mathbf{x})] n_a(\mathbf{x}) \sigma_{ab}^{*q}(\mathbf{x},\xi) \, dS + \int_{\Gamma_s} [D_p u_q(\xi) - (D_p u_q)(\mathbf{x})] n_a(\mathbf{x}) \Sigma_{abpq}^{*}(\mathbf{x},\xi) \, dS + \int_{\Omega_s} f_q(\xi) n_a(\mathbf{x}) \sigma_{ab}^{*q}(\mathbf{x},\xi) \, d\Omega \tag{33}$$

The derivation of non-hypersingular traction BIE was reported in [Han and Atluri (2003a)]. This generalized MLPG/LBIE formulations have been derived with details in [Han and Atluri (2004)].

On the contrast, the conventional MLPG/LBIE methods use a "companion solution", $\tilde{u}_i^p(\mathbf{x},\xi)$, to get rid of the unknown traction in the first term of Eq. (30). The companion solution is associated with the fundamental solution and the local test sub-domain. It is defined as the solution to the following equations:

$$\begin{cases} \tilde{\sigma}_{ij,j}^p = 0 & on \quad \Omega_s \\ \tilde{u}_i^p = u_i^{*p} & on \quad \partial\Omega_s \end{cases} \tag{34}$$

For a 3D problem, it is given for a spherical local sub-domain, with a radius of r_0, as:

$$\tilde{u}_i^p(\mathbf{x},\xi) = \frac{1}{16\pi\mu(1-\upsilon)r_0}[(3-4\upsilon)\delta_{ip} + \frac{r^2}{r_0^2}r_{,i}r_{,p} + \frac{3-2\upsilon}{2(2-3\upsilon)}(1-\frac{r^2}{r_0^2})\delta_{ip}] \tag{35a}$$

$$\tilde{\sigma}_{ij}^p(\mathbf{x},\xi) = \frac{1}{8\pi(1-\upsilon)r_0^2}\,\frac{(1+\upsilon)r}{2(2-3\upsilon)r_0} (4\delta_{ij}r_{,p} - \delta_{ip}r_{,j} - \delta_{jp}r_{,i}) \tag{35b}$$

By taking the companion solution in Eq. (35) as the test functions, the local weak form can be written as:

$$\int_{\Gamma_s} t_i(\xi)\tilde{u}_i^p(\mathbf{x},\xi)\,dS - \int_{\Gamma_s} u_i(\xi)\tilde{t}_i^p(\mathbf{x},\xi)\,dS + \int_{\Omega_s} f_i(\xi)\tilde{u}_i^p(\mathbf{x},\xi)\,d\Omega = 0 \tag{36}$$

One may also define a solution, $\tilde{u}_i^{*p}(\mathbf{x},\xi)$, as:

$$\tilde{u}_i^{*p}(\mathbf{x},\xi) = u_i^{*p}(\mathbf{x},\xi) - \tilde{u}_i^p(\mathbf{x},\xi) \tag{37}$$

and rewrite the local weak with them as the test functions for a spherical local sub-domain, with the consideration of Eq. (34):

$$\int_{\Gamma_{st}} \bar{t}_i(\xi)\tilde{u}_i^{*p}(\mathbf{x},\xi)\,dS + \int_{\Gamma_{su}} t_i(\xi)\tilde{u}_i^{*p}(\mathbf{x},\xi)\,dS - \int_{\Gamma_s} [u_i(\xi)-u_i(\mathbf{x})]\tilde{t}_i^{*p}(\mathbf{x},\xi)\,dS + \int_{\Omega_s} f_i(\xi)\tilde{u}_i^{*p}(\mathbf{x},\xi)\,d\Omega = 0 \tag{38}$$

Eq. (38) is conventional meshless local weak form as LBIE, which is restricted to the spherical local sub-domain only [Atluri, Sladek, Sladek and Zhu (2000)]. The advantage is that there are no unknown tractions to be evaluated on the part of the boundary of the local sub-domain which is inside the solution domain. The disadvantage is that the local sub-domain is limited by the companion solution. It needs the special numerical techniques for the strong singular integrals. For the present LBIE formulations in Eqs. (30) and (33), there are no strong singular integrals as they are fully regularized. They have no restrictions in choosing the local sub-domain, which could be spheres or polyhedrons with more details in the following section for 3D problems. Another difference is the use of the unknown traction variables. In the conventional LBIEs, the unknown variables are displacements, with the tractions as the derived one. Sellountos and Polyzos (2003) introduced the unknown traction variables to the displacement LBIE, whose application is limited. However, the presented LBIEs for displacements and tractions can be used together for solving problems in which the tractions need to be unknown variables, such as those with cracks, contact and material interfaces. It makes the LBIE more general and flexible. These non-hyper-singular BIEs have also been successfully applied together for acoustic problems [Qian, Han, Ufimtsev and Atluri (2004)].

4 Discretization and numerical implementation

4.1 MLPG/Symmetric: using the shape function as the test function and collocation method for the essential boundary conditions for LSWF

Let us apply the local symmetric weak form in Eq. (24) on the local 3D sub-domain Ω_s, centered on each nodal point $\mathbf{x}^{(I)}$. If its ith degree of freedom (DOF) is not prescribed, i.e., $u_i^{(I)} \notin \Gamma_{su}$, or the node is inside the domain, one may take the shape function of node k in Eq.

(7), $\Phi^{(I)}(\mathbf{x})$, as the test function. In addition, the local-domain is chosen as the same as the support domain of the node, Eq. (24) can be simplified for $u_i^{(I)}$ as:

$$\int_{\Omega_s} \sigma_{ij}\Phi^{(I)}_{,j}d\Omega - \int_{\Gamma_{su}} t_i\Phi^{(I)}d\Gamma = \int_{\Gamma_{st}} \overline{t}_i\Phi^{(I)}d\Gamma + \int_{\Omega_s} f_i\Phi^{(I)}d\Omega \tag{39}$$

in which the following condition has been used:

$$\Phi^{(I)}(\mathbf{x}) = 0 \quad \text{for} \quad \forall \mathbf{x} \in L_s \tag{40}$$

If the ith DOF belongs to the displacement boundary, i.e., $u_i^{(I)} \in \Gamma_{su}$, one may take the Derac's delta function as the test function and obtain the corresponding local weak form from Eq. (24):

$$\alpha u_i(\mathbf{x}^{(I)}) = \alpha\overline{u}_i(\mathbf{x}^{(I)}) \tag{41}$$

By taking the approximation in Eq. (6) and the constitute relations in Eq. (19), Eqs. (39) and (41) are ready for numerical implementation, labeled as MLPG6 in [Atluri(2004)]. This method has the following properties:

The system matrix is symmetric.

The system matrix is sparse and banded.

4.2 MLPG/Heaviside: using Heaviside step function as the test function and collocation method for the essential boundary conditions for LSWF

Similar to MLPG/Symmetric, a Heaviside step function is used as the test function for the nodes on the natural boundary or inside the domain, i.e., $u_i^{(I)} \notin \Gamma_{su}$. One may simplify Eq. (24) for $u_i^{(I)}$ as:

$$-\int_{L_s} t_i d\Gamma - \int_{\Gamma_{su}} t_i d\Gamma = \int_{\Gamma_{st}} \overline{t}_i d\Gamma + \int_{\Omega_s} f_i d\Omega \tag{42}$$

For the ith DOF belongs to the displacement boundary, i.e., $u_i^{(I)} \in \Gamma_{su}$, the similar equation can be obtained by taking the Derac's delta function as the test function for MLGP/Symmetric as:

$$\alpha u_i(\mathbf{x}^{(I)}) = \alpha\overline{u}_i(\mathbf{x}^{(I)}) \tag{43}$$

By taking the approximation in Eq. (6) and the constitute relations in Eq. (19), Eqs. (42) and (43) are ready for numerical implementation. This method has the following properties:

The system matrix is unsymmetric.

The system matrix is sparse and banded.

Theoretically, the shapes of the sub-domains can be chosen arbitrarily, including spheres, cubes, polyhedrons, ellipsoids and so on. The practical shapes may be restricted to those have a piece-wise surface. It is discussed with more details in the next section.

4.3 MLPG/LBIE: using the fundamental solution as the test function for LUSWF (LBIE)

Most LBIE work in literatures is based on Eq. (38) for 2D problems, with the use of either companion solutions [Atluri, Sladek, Sladek and Zhu (2000), Sladek, Sladek and Zhang (2003), Sellountos and Polyzos (2003)], or cut-off functions [Mikhailov (2002)]. The local sub-domain needs to be chosen as a circle centered at the nodal point in question. Then the conventional quadrature schemes are used for the integrals over the circle. This idea may not work for 3D problems, by choosing a sphere as a simple extension, because integrals for LBIE need to be performed over the surface of the local sub-domain. In contrast, Eq. (30) has no such kind of restriction in choosing the local sub-domain. In addition, Eq. (30) contains no strong singularities, and the weakly singular integrals can be easily evaluated by using the conventional Gauss qradrature scheme over the piece-wisely surface. For the nodes on the global boundary, the weak singularities can be cancelled by the Jacobian of the coordinate transforms, in which the conventional Gauss quadrature is still applicable.

By taking the meshless approximation in Eq. (6), the displacements, tractions and body forces can be expressed as:

$$u_i(\xi) = \sum_{j=1}^{N} \Phi^{(J)}(\xi)u_i^{(J)} \tag{44a}$$

$$t_i(\xi) = \sum_{J=1}^{N} [\lambda n_i(\xi)\Phi^{(J)}_{,j}(\xi)u_j^{(J)} + \mu n_j(\xi)\Phi^{(J)}_{,j}(\xi)u_i^{(J)} + \mu n_j(\xi)\Phi^{(J)}_{,i}(\xi)u_j^{(J)}] \tag{44b}$$

$$f_i(\xi) = \sum_{J=1}^{N} \Phi^{(J)}(\xi) f_i^{(J)} \tag{44c}$$

in which the constitute relations in Eq. (19) is used, and N is the number of the nodes in the solution domain. One may discretize the LBIE in Eq. (30), corresponding to node I's p-th displacement, $u_p^{(I)}$, as:

$$\begin{aligned}
&\sum_{J=1}^{N} u_j^{(J)} \int_{L_s} [\lambda u_i^{*p}(\mathbf{x},\xi) n_i(\xi) \Phi_{,j}^{(J)}(\xi) \\
&\qquad + \mu u_j^{*p}(\mathbf{x},\xi) n_i(\xi) \Phi_{,i}^{(J)}(\xi) \\
&\qquad + \mu u_i^{*p}(\mathbf{x},\xi) n_j(\xi) \Phi_{,i}^{(J)}(\xi)] d\Gamma \\
&- \sum_{J=1}^{N} (u_i^{(J)} - \delta_{ip} u_p^{(I)}) \int_{\Gamma_s} t_i^{*p}(\mathbf{x},\xi) \Phi^{(J)}(\xi) d\Gamma \\
&= - \int_{\Gamma_s} \bar{t}_i(\xi) u_i^{*p}(\mathbf{x},\xi)\, dS \\
&- \int_{\Omega_s} [\sum_{J=1}^{N} f_i^{(J)} \Phi^{(J)}(\xi)] u_i^{*p}(\mathbf{x},\xi)\, d\Omega
\end{aligned} \tag{45}$$

The local sub-domains for this method are also chosen as the polyhedrons centered at each node, defined in the following section.

5 The shape of 3D local sub-domain

For MLPG/Symmetric and MLPG/Heaviside, the tractions are included in the integrals which need to be performed over the surface of the local sub-domain. By definition, the tractions, $t_i \equiv \sigma_{ij} n_j$, contain the normal $\mathbf{n}$ to the surface. It is seen that, in defining the unit normal on a 3-D spherical surface, the trigonometric functions are involved. It is well known that the conventional numerical quadrature schemes are designed for polynomials, and are not efficient for trigonometric functions. It is well known that a 2-point Gauss quadrature evaluates $\int_0^1 x^3\, dx$ accurately. However, the numerical experiments show that, it gives an error of about 0.07% when a 4-point Gauss quadrature is used to evaluate one dimensional integral $\int_0^1 x^3 \sin 2\pi x\, dx$ over a 2D circle, in which only one trigonometric function is involved. It gives a higher error of 0.15% for a 4x4 point Gauss quadrature to evaluate a double integral $\int_0^1 \int_0^1 x^3 y^3 \sin 2\pi x \sin 2\pi y\, dxdy$ over a spherical surface, and an error of 1.5×10^{-5} for

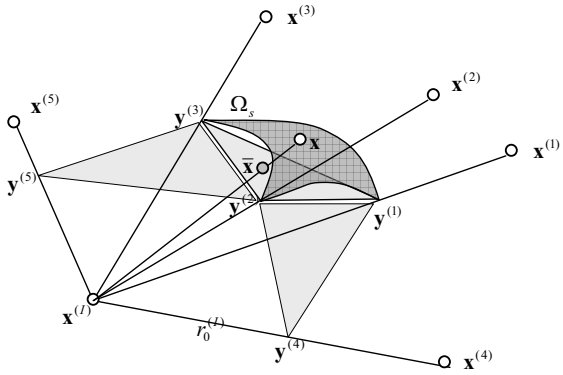

Figure 2 : a local sub-domain around point $\mathbf{x}$

a 6x6 point Gauss quadrature. However, the shape functions constructed here are more complicated than simple monomials. For 2D problems, such numerical errors may be controlled by simply increasing the order of Gauss quadrature scheme, or subdividing the domain of integration into small segments for better accuracy. It has been reported that the subdivision algorithm is much more efficient than those the integration is performed over the entire domain with a large number of integration points [Atluri, Kim and Cho (1999), Sellountos and Polyzos (2003)]. The integration over the entire domain is tediously inefficient for 3D problems, as the high order Gauss quadrature is required even for passing patch tests. In the present implementation, the piece-wise polyhedron is defined for each node in the following way, to subdivide the local spherical domain for simplifying the numerical quadrature and improving the accuracy.

Consider node I at $\mathbf{x}^{(I)}$, one may determine the radius of a local sphere centered at node I, denoted by $r_0^{(I)}$:

$$r_0^{(I)} = \alpha \min\{\left\|\mathbf{x}^{(I)} - \mathbf{x}^{(K)}\right\|, K = 1,2,...,n \text{ and } K \neq I\} \tag{46}$$

where α is a constant and greater than 0 and less than 1. It is chosen as 0.75 in the present study.

In addition, if node I is inside the solution domain but close to the global boundary, a smaller radius may be used so that the local sphere has no intersection with the global boundary. In other words, the local test subdomains of all internal nodes are restricted inside the solution domain, and their local boundaries are also inside

the solution domain. Therefore, the numerical implementation becomes much simpler, because the essential and natural boundary conditions appear in the integrals of the nodes on the global boundary only.

With the use of the local radius, $r_0^{(I)}$, one may define a minimum subset of nodes, $\{\mathbf{x}^{(J)}\}$, $(J = 1,2,...,m)$, by which the local sphere is covered. By drawing a line from node I to node J, a point can be obtained at the intersection between the line and the local sphere, denoted by $\mathbf{y}^{(J)}$. One may use Delaunay triangulation algorithm to triangulate the local spherical surface through $\{\mathbf{y}^{(J)}\}$, $(J = 1,2,...,m)$. Then a set of 3-node triangles are obtained which define a local polyhedron, as shown in Figure 2. Then the local spherical sub-domain for node I can be sub-divided into pieces through these triangles. The integration can be performed over the triangles by mapping the point $\overline{\mathbf{x}}$ back to the point $\mathbf{x}$ on the spherical surface. For a surface integration, one may write the mapping relationship between points $\overline{\mathbf{x}}$ and $\mathbf{x}$, as

$$\begin{aligned} &\theta(\mathbf{x}) = \theta(\overline{\mathbf{x}}), \quad \varphi(\mathbf{x}) = \varphi(\overline{\mathbf{x}}) \\ &dS(\mathbf{x}) = dS(\overline{\mathbf{x}})[\frac{r_0^{(I)}}{\|\overline{\mathbf{x}}-\mathbf{x}^{(I)}\|}]^2 \end{aligned} \tag{47}$$

In addition, the corresponding tetrahedron can be defined for each triangle by adding node I as the 4-th vertex and then mapping back to the corresponding cone. Thereafter, all integrals over the local surface can be mapped over the triangles, and the local sub-domain integrals over the tetrahedrons, using very simple Gaussian quadrature.

6 Numerical Experiments

Several problems in three-dimensional linear elasticity are solved, to illustrate the effectiveness of the present method. The numerical results of the present methods, as applied to problems in 3D elasto-statics, specifically (i) a cube, (ii) a hollow sphere, (iii) cantilever beam, (iv) concentrated load on a semi-infinite space (Boussinesq Problem), are discussed.

6.1 Cube under uniform tension

The first example is that of a standard patch test, shown in Figure 3. A cube under the uniform tension is considered. The material parameters are taken as $E = 1.0$, and $\nu = 0.25$. The cube is modeled with 27 nodes, including one node in the center of cube and 9 nodes for each of the faces. Two nodal configurations are used for the testing purpose: one is regular and another is irregular, as shown in Figure 3. In the patch tests, the uniform tension stress is applied on the upper face and the proper displacement constraints are applied to the lower face.

The satisfaction of the patch test requires that the displacements are linear on the lateral faces, and are constant on the upper face; and the stresses are constant on all faces. It is found that the present methods pass the patch tests. The maximum numerical errors are limited by the computer for two nodal configurations.

6.2 3D Lamé problem

The 3D Lame problem consists of a hollow sphere under internal pressure, as illustrated in Figure 4. The geometry is defined with the inner and outer radius of 1.0 and 4.0, respectively. The Young's modulus is chosen as $E = 1.0$ and the Poisson ratio$\nu = 0.25$. The internal pressure $p = 1.0$ is applied. With the consideration of the symmetric load and boundary conditions, only one eighth of the sphere is models with the proper boundary conditions. The non-uniform nodal configuration of 333 nodes is used, as shown in Figure 5.

The radial displacement field is given in [Timoshenko & Goodier (1976)],

$$u_r = \frac{pRa^3}{E(b^3-a^3)}\left[(1-2v)+(1+v)\frac{b^3}{2R^3}\right] \tag{48}$$

The radial and tangential stresses are

$$\begin{aligned} \sigma_r &= \frac{pa^3(b^3-R^3)}{R^3(a^3-b^3)} \\ \sigma_\theta &= \frac{pa^3(b^3+2R^3)}{2R^3(b^3-a^3)} \end{aligned} \tag{49}$$

The displacements are shown in Figure 6, and are compared with the analytical solution. As shown in Figure 7, the radial and tangential stresses are compared with the analytical solution. They agree with each other very well.

6.3 Cantilever beam

The performances of the present MLPG formulations are also evaluated, using the cantilever beam problem under

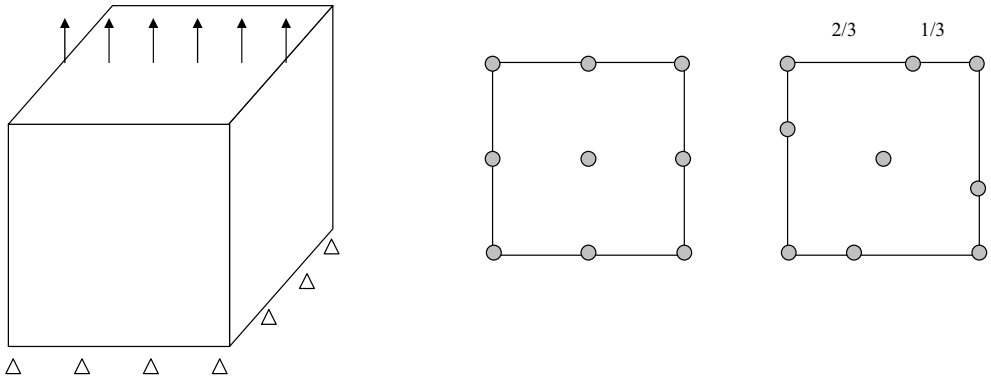

Figure 3 : A cube under uniform tension, and two nodal configurations

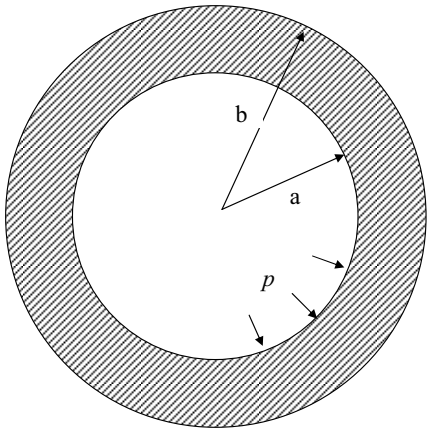

Figure 4 : A hollow sphere under internal pressure (Lame problem)

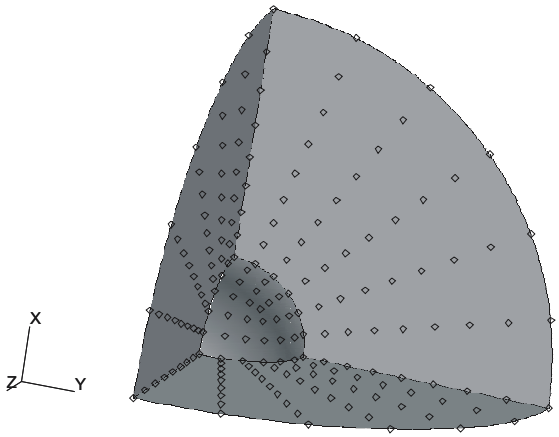

Figure 5 : nodal configuration for one-eighth hollow sphere

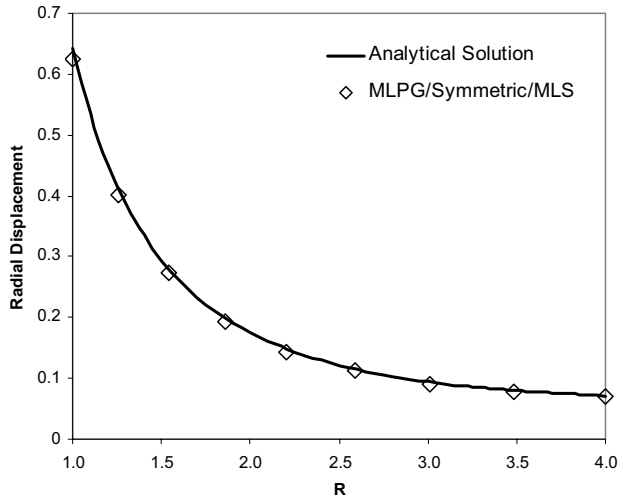

Figure 6 : Radial displacement for the Lame problem

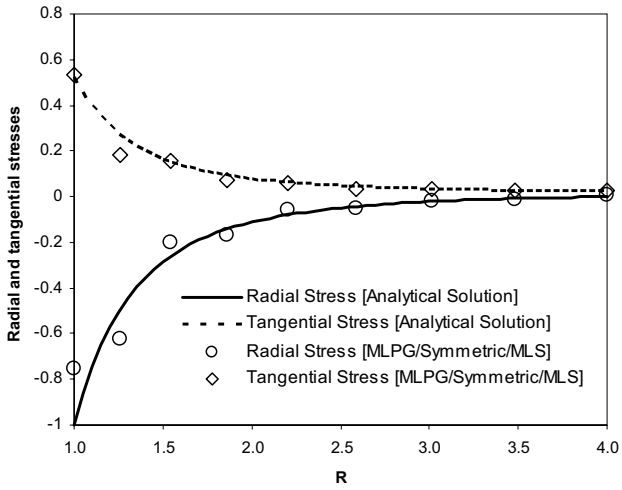

Figure 7 : Radial and tangential stresses for the Lame problem

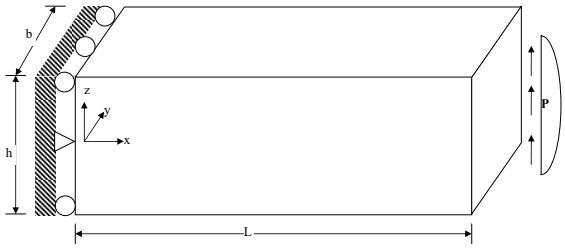

Figure 8 : A cantilever beam with an end load

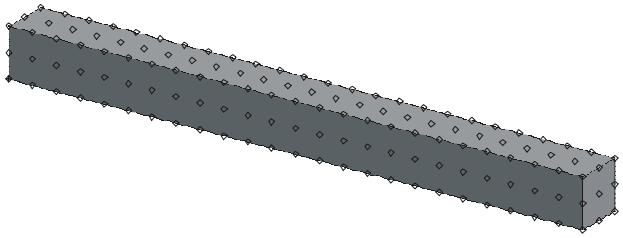

Figure 9 : nodal configuration for a cantilever beam with 225 nodes

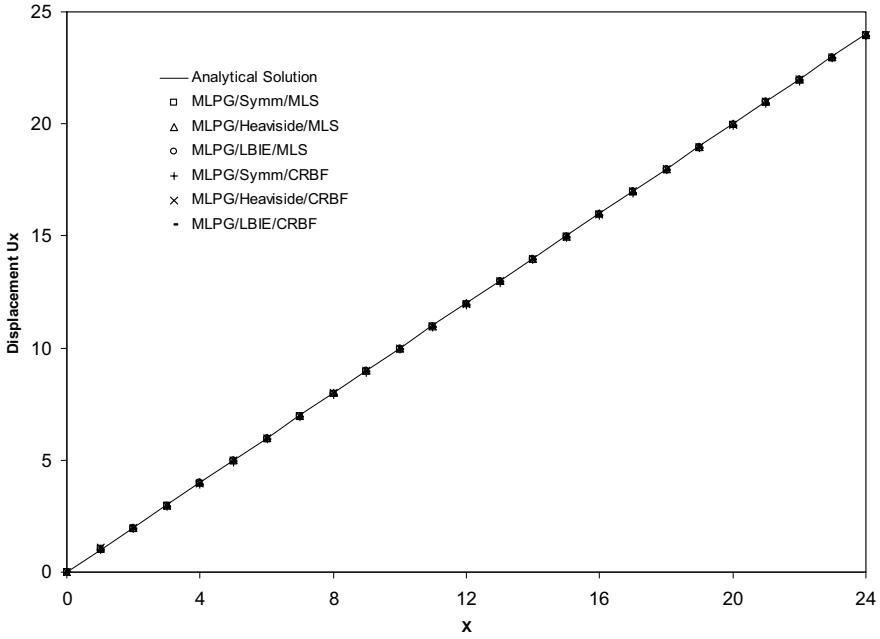

Figure 10 : Tension deformation for a cantilever beam under a uniform tension: nodal distance d=1.0, support size R = 2.6

a transverse load, shown in Figure 8, for which the following exact solution is given in Timoshenko and Goodier (1970):

$$u_x = -\frac{P(1-\overline{\upsilon}^2)}{6b\overline{E}I}(y-\frac{h}{2})[3x(2L-x)+\frac{2-\overline{\upsilon}}{1-\overline{\upsilon}}y(y-h)]$$
$$u_y = \frac{P(1-\overline{\upsilon}^2)}{6b\overline{E}I}[x^2(3L-x)+\frac{3\overline{\upsilon}}{1-\overline{\upsilon}}(L-x)(y-\frac{h}{2})^2 + \frac{4+\overline{\upsilon}}{4-4\overline{\upsilon}}h^2x] \quad (50)$$

where I is the bending stiffness of the plate, as,

$$I = \frac{h^3}{12} \quad (51)$$

and

$$\overline{E} = \begin{cases} E & \\ \frac{1+2\upsilon}{(1+\upsilon)^2}E & \end{cases} \quad \text{and} \quad \overline{\upsilon} = \begin{cases} \upsilon & \text{for plane strain} \\ \frac{\upsilon}{1+\upsilon} & \text{for plane stress} \end{cases} \quad (52)$$

The corresponding stresses are

$$\begin{aligned}\sigma_x &= -\frac{P}{bI}(L-x)(y-\frac{h}{2})\\ \sigma_y &= 0\\ \sigma_{xy} &= -\frac{P}{2bI}y(y-h)\end{aligned} \tag{53}$$

The problem is solved for the plane stress case with $P=1$, $E=1$, $b=h=2$, $L=24$ and $\upsilon=0.25$. Regular uniform nodal configurations with nodal distances, d, of 2.0, 1.0, 0.5, 0.25 and 0.125 are used, as Figure 9 shows the configuration with a nodal distance of 1.0. The number of nodes are 52, 225, 1225, 7857 and 55777, respectively. For the comparison purpose, FE meshes are also constructed from the nodal configurations by using the standard Hex 8 element.

First, a uniform tension load is applied to the free end of the cantilever beam. A linear deformation field is expected for this simple loading. The problem is solved by using the three MLPG methods with both the MLS and CRBF approximations. The numerical results of the tension deformation are shown in Figure 10, which agree with the analytical solution well. The maximum relative error is less than 0.25%, as listed in Figure 11.

The MLPG/LBIE is used to solve the beam under the transverse load. The results with the MLS approximation with a linear basis are shown in Figure 12, with the stream line from the exact solution. It can be seen that the results are well approximated by the MLPG/LBIE method with a nodal distance of 0.5, as compared to the analytical solution. The results from the MLPG/Symmetric method are shown in Figure 13. This method gives the better results even with a nodal distance of 1.0. The linear basis yields almost the same results as the quadratic basis for the MLS approximation. The convergence with nodal refinement of the MLPG/Symmetric method is studied for this problem. The results of relative errors are shown in Figure 14. The relative errors of the FEM with the conventional Hex8 elements are also shown in Figure 14. It shows a faster convergence rate of the present MLPG method than the FEM.

6.4 A concentrated load on a semi-infinite space (Boussinesq problem)

The Boussinesq problem can simply be described as a concentrated load acting on a semi-infinite elastic medium with no body force, as shown in Figure 15. This problem was solved by using MLPG/Heaviside [Li, Shen, Han and Atluri (2003)] and MLPG/BIE [Han and Atluri (2003)b]. *In Li, Shen, Han, and Atluri (2003), the problem was simplified, somewhat, by carving out a sphere of a small radius, at the point of application of the concentrated load, and applying only displacement boundary conditions (corresponding to the analytical solution), on the inner surface of this small sphere.* In the present paper, the MLPG methods are used to solve this problem, by directly applying the point load itself, to show the capability of the MLPG methods for the strong singularities. A quarter of a half sphere with a radius of 10 is used to simulate the semi-infinite space, with the consideration of the symmetrical boundary conditions. It is modeled with a nodal configuration, as shown in Figure 16a, containg 1067 nodes. For comparison purposes, a mesh for the FEM is also constructed from the same nodes by using tetrahedral elements. In addition, a finer tetrahedral mesh for FEM is also created with 4869 nodes, as shown in Figure 16b. Young's modulus and Poisson's ratio are chosen to be 1.0 and 0.25, respectively.

The exact displacement field within the semi-infinite medium is given in [Timoshenko & Goodier (1976)],

$$\begin{aligned}u_r &= \frac{(1+\nu)P}{2E\pi R}\left[\frac{zr}{R^2}-\frac{(1-2\nu)r}{R+z}\right]\\ u_w &= \frac{(1+\nu)P}{2E\pi R}\left[\frac{z^2}{R^2}+2(1-\nu)\right]\end{aligned} \tag{54}$$

where u_r is the radial displacement, and u_w is the vertical one, R is the distance to the loading point, r is the projection of R on the loading surface.

The theoretical stress field is:

$$\begin{aligned}\sigma_r &= \frac{P}{2\pi R^2}\left[-\frac{3r^2z}{R^3}+\frac{(1-2\nu)R}{R+z}\right]\\ \sigma_\theta &= \frac{(1-2\nu)P}{2\pi R^2}\left[\frac{z}{R}-\frac{R}{R+z}\right]\\ \sigma_z &= -\frac{3Pz^3}{2\pi R^5}\\ \tau_{zr} &= \tau_{rz} = -\frac{3\,\mathrm{Pr}\,z^2}{2\pi R^5}\end{aligned} \tag{55}$$

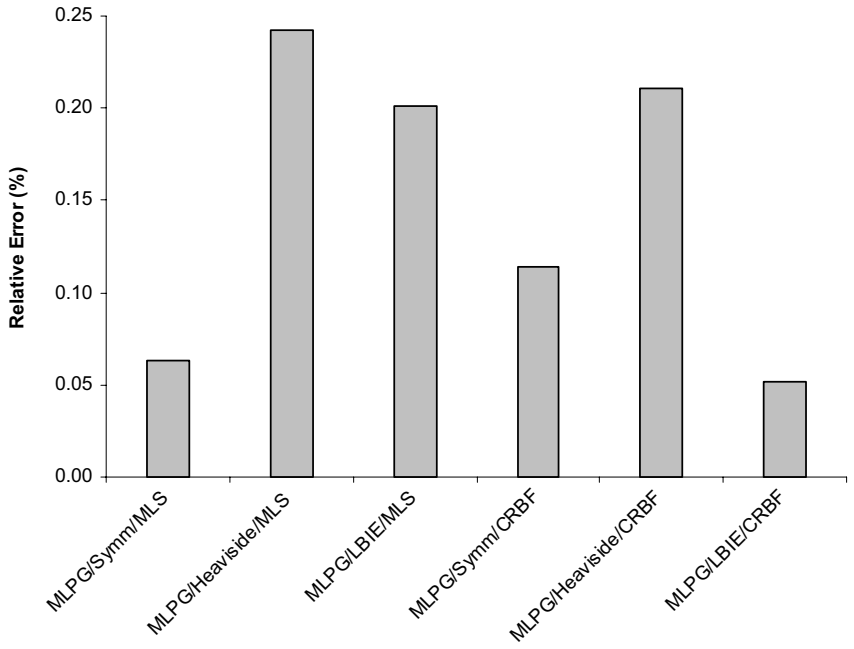

Figure 11 : Relative errors of the tension deformation for a cantilever beam under a uniform tension

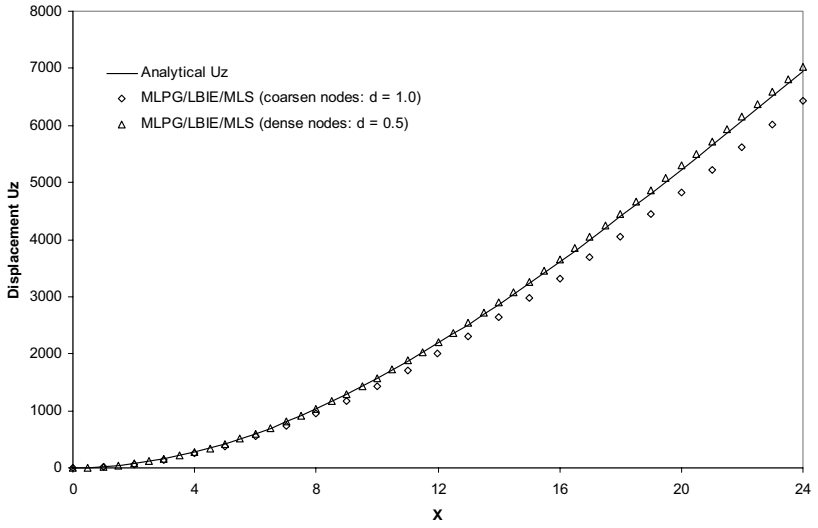

Figure 12 : Effect of the nodal distance on the transverse deformation of a cantilever beam for MLPG/LBIE

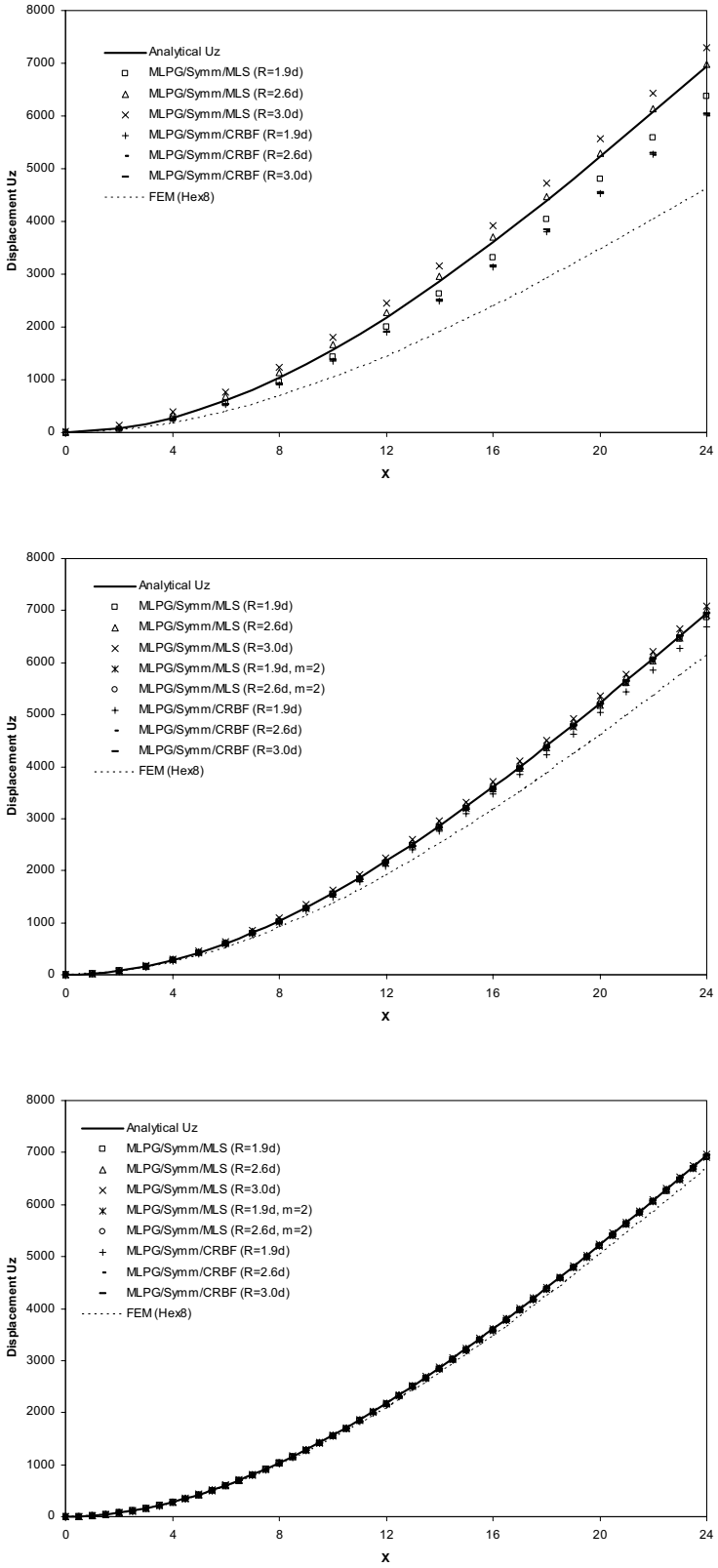

Figure 13 : Effect of the nodal distance and support size on the transverse deformation of a cantilever beam: a) d = 2.0; b) d=1.0; c) d=0.5

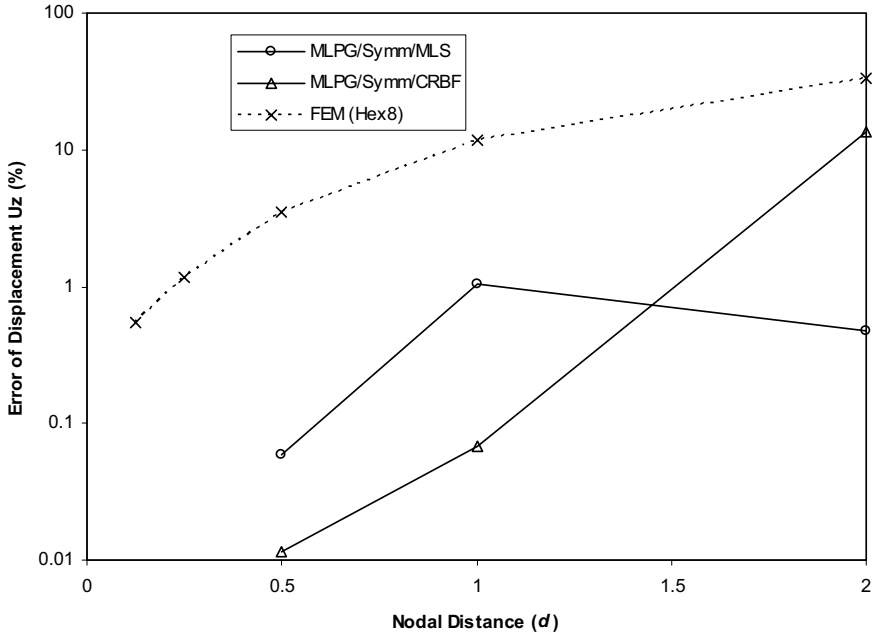

Figure 14 : Relative errors of the transverse deformation for a cantilever beam vs the nodal distance

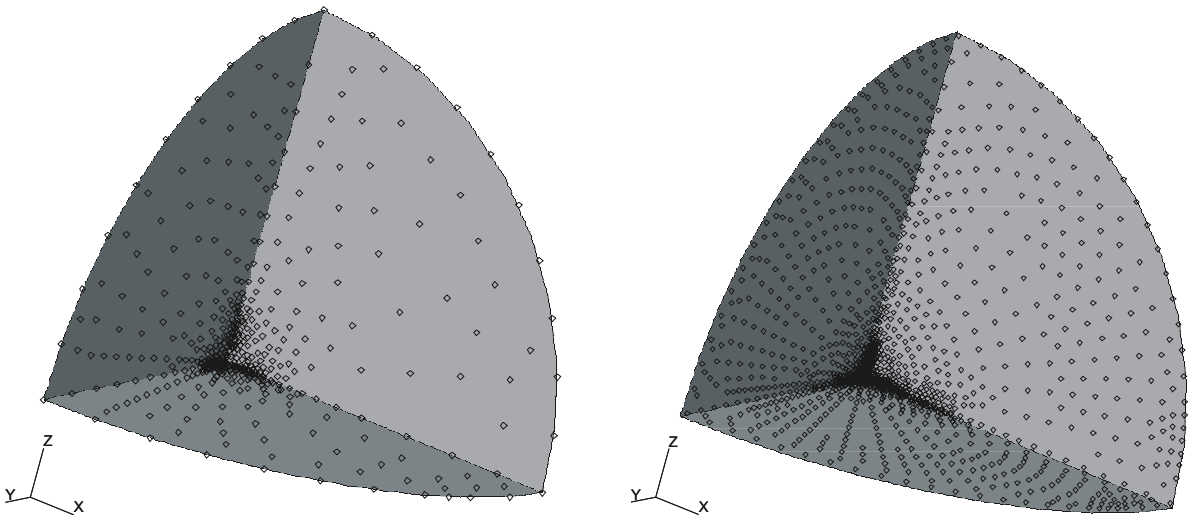

Figure 16 : two nodal configurations for the Boussinesq Problem:(a) 1067 nodes, and (b) 4869 nodes

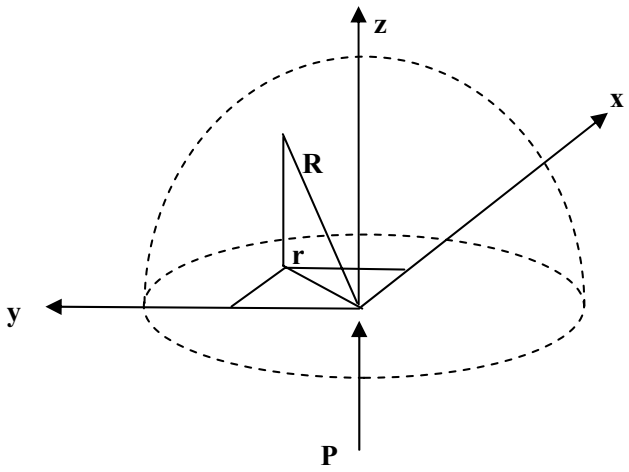

Figure 15 : A concentrated load on a semi-infinite space (Boussinesq Problem)

It is clear that the displacements and stresses are strongly singular and approach to infinity; with the displacement being $O(1/R)$ and the stresses being$O(1/R^2)$.

The vertical displacement u_w along the z-axis is shown in Figure 17. The radial stresses along the Z and Y axes are shown in Figure 18 and Figure 19. The analytical solution for the displacement and stress are plotted on the same figures for comparison purpose. The results show that the present MLPG method gives much better results than the FEM method, when the same nodal configuration is used. The FEM achieves the same accuracy, as the present MLPG methods, only when a 4-time finer mesh is used. For this finer mesh, it takes a much longer CPU time for the FEM to solve the problem, along with more system resources. The CPU Time and the used system memory are shown in 6.4. For the same accuracy, the MLPG method takes lesser CPU time, as well as lesser system resources, than the FEM.

7 Closure

Three Meshless Local Petrov Galerkin (MLPG) methods are developed for 3D static problems, based on the local symmetric and unsymmetric weak forms. The MLS and CRBF approximations are used for constructing the shape functions from the scattered points. A novel method has also been developed to define the local subdomains from the polyhedrons for the evaluation of the integrals. The numerical results demonstrate the advantages of the present MLPG methods over the Finite element method, including the higher accuracy, and the smoother stress fields. Convergence studies in the numerical examples show that the present methods possess an excellent rate of convergence for both the unknown variable and its derivatives, which are even faster than the conventional FEM. The much lesser number of nodes required in the MLPG methods, to obtain the same accuracy, as compared to the FEM, in static 3_D elasticity problems, is demonstrated. *It also leads to the conclusion, that the present MLPG methods are even more efficient for dynamic problems, while using explicit time-integration schemes, because only the simple matrix multiplication operations are involved, instead of the matrix reversion as in the static problems.* This is discussed in detail, in a companion paper.

Acknowledgement: The results presented in this paper were obtained during the course of investigations supported by the United States Army, under the SBIR Contract, Number: W911NF-04-C-0022. ZH and SNA gratefully acknowledge the fruitful discussions with, and the encouragement received from, Dr. Ellen Segan of the US Army Research Office, during the performance of this research.

References

Atluri, S.N (2004): *The Meshless Local Petrov-Galerkin (MLPG) Method for Domain & Boundary Discretizations*, Tech Science Press, 700 pages.

Atluri, S. N.; Han, Z. D.; Shen, S. (2003): Meshless Local Patrov-Galerkin (MLPG) approaches for weakly-singular traction & displacement boundary integral equations, CMES: *Computer Modeling in Engineering & Sciences*, vol. 4, no. 5, pp. 507-517.

Atluri, S.N., Kim, H.G., Cho, J.Y. (1999): A Critical Assessment of the Truly Meshless Local Petrov Galerkin (MLPG) and Local Boundary Integral Equation (LBIE) Methods, *Computational Mechanics*, 24:(5), pp. 348-372.

Atluri S.N., Sladek J., Sladek V., Zhu T. (2000): The local boundary integral equation (LBIE) and it's meshless implementation for linear elasticity, *Computational Mechanics*, vol. 25 nos.2-3, pp. 180-198.

Atluri, S. N.; Shen, S. (2002a): The meshless local Petrov-Galerkin (MLPG) method. Tech. Science Press,

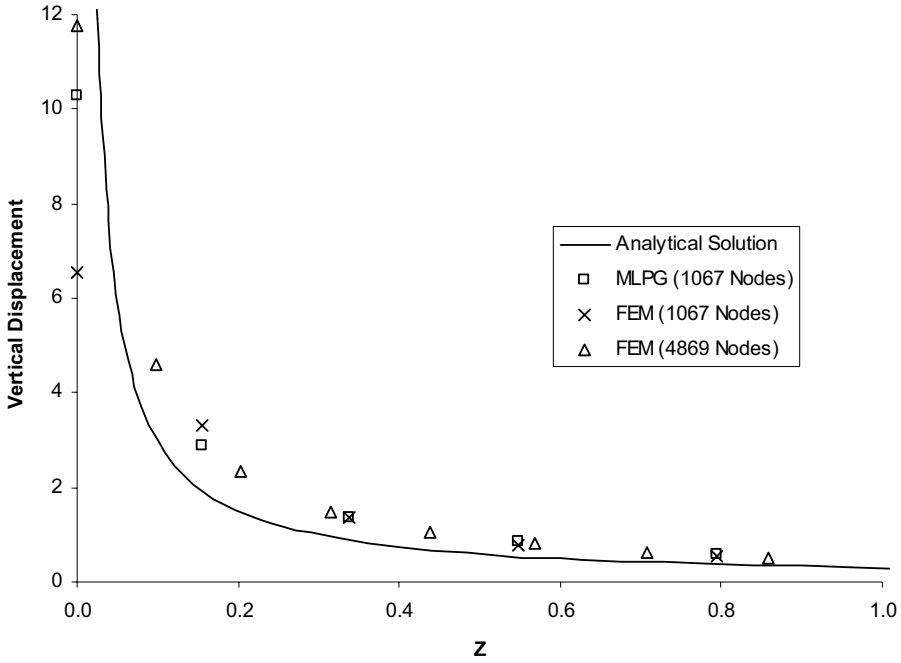

Figure 17 : Vertical displacement along z-axis for the Boussinesq problem

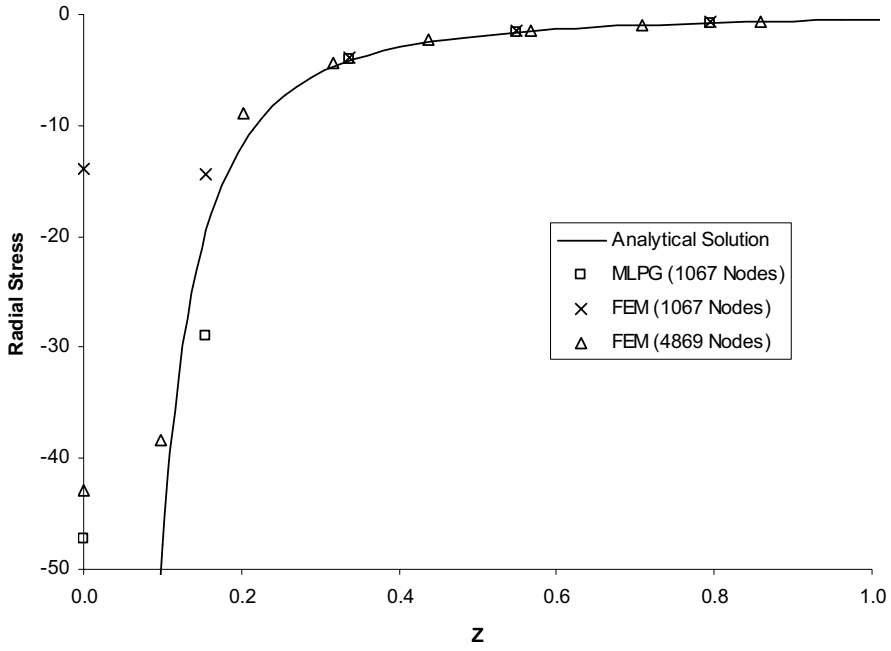

Figure 18 : Radial stress along z-axis for the Boussinesq problem

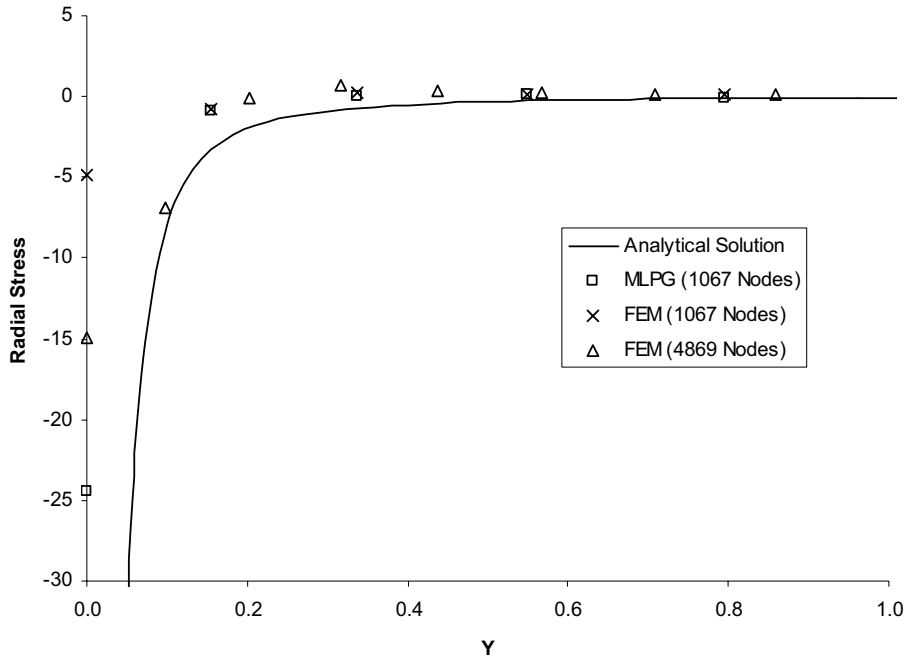

Figure 19 : Radial stress along y-axis for the Boussinesq problem

Table 1 : CPU time and used memory for MLPG and FEM to solve Boussinesq problem

Method	Number of Node	Max Disp.	Max Stress	CPU Time (Second)	Memory (MB)
MLPG	1067	10.3	47.2	56.2	20
FEM	1067	6.5	13.9	3.2	5
FEM	4869	11.8	42.9	61.8	91

440 pages.

Atluri, S. N.; Shen, S. (2002b): The meshless local Petrov-Galerkin (MLPG) method: A simple & less-costly alternative to the finite element and boundary element methods. CMES: *Computer Modeling in Engineering & Sciences*, vol. 3, no. 1, pp. 11-52

Atluri, S. N.; Zhu, T. (1998): A new meshless local Petrov-Galerkin (MLPG) approach in computational mechanics. *Computational Mechanics.*, Vol. 22, pp. 117-127.

Golberg, M. A., Chen, C. S., Bowman, H. (1999): Some recent results and proposals for the use of radial basis functions in the BEM, *Engineering Analysis with Boundary Elements*, vol. 23, pp. 285-296.

Han. Z. D.; Atluri, S. N. (2003a): On Simple Formulations of Weakly-Singular Traction & Displacement BIE, and Their Solutions through Petrov-Galerkin Approaches, CMES: *Computer Modeling in Engineering & Sciences*, vol. 4 no. 1, pp. 5-20.

Han. Z. D.; Atluri, S. N. (2003b): Truly Meshless Local Petrov-Galerkin (MLPG) Solutions of Traction & Displacement BIEs, CMES: *Computer Modeling in Engineering & Sciences*, vol. 4 no. 6, pp. 665-678.

Han. Z. D.; Atluri, S. N. (2004): Generalized MLPG/LBIE Formulations For Meshless Domain Discretizations, CMC: *Computers, Materials,& Continua*, submitted.

Li, Q.; Shen, S.; Han, Z. D.; Atluri, S. N. (2003): Application of Meshless Local Petrov-Galerkin (MLPG) to Problems with Singularities, and Material Discontinuities, in 3-D Elasticity, CMES: *Computer Modeling in Engineering & Sciences*, vol. 4 no. 5, pp. 567-581.

Mikhailov, S. E. (2002): Localized boundary-domain integral formulations for problems with variable coefficients. *Engn. Anal. Bound. Elem.*, vol. 26, pp. 681-690.

Okada, H.; Rajiyah, H.; Atluri, S. N. (1989)a: A Novel Displacement Gradient Boundary Element Method for Elastic Stress Analysis with High Accuracy, *J. Applied Mech*., April 1989, pp. 1-9.

Okada, H.; Rajiyah, H.; Atluri, S. N. (1989)b: Non-hyper-singular integral representations for velocity (displacement) gradients in elastic/plastic solids (small or finite deformations), *Comp. Mech.*, vol. 4, pp. 165-175.

Qian, Z.Y.; Han, Z.D.; Ufimtsev, P.; Atluri, S.N. (2004): Non-Hyper-Singular Boundary Integral Equations for Acoustic Problems, Implemented by the Collocation-Based Boundary Element Method, CMES: *Computer Modeling in Engineering & Sciences*, vol. 6 no. 2, pp. 133-144.

Sellountos, E. J.; Polyzos, D. (2003): A MLPG (LBIE) method for solving frequency domain elastic problems, *CMES: Computer Modeling in Engineering & Sciences*, vol. 4, no. 6, pp. 619-636

Sladek, J.; Sladek, V.; Zhang, C. (2003): Application of Meshless Local Petrov-Galerkin (MLPG) Method to Elastodynamic Problems in Continuously Nonhomogeneous Solids, *CMES: Computer Modeling in Engineering & Sciences*, vol. 4, no. 6, pp. 637-648.

Timoshenko, S. P.; Goodier, J. N. (1976): Theory of Elasticity, 3^{rd} edition, McGraw Hill.

Zhu, T., Zhang, J.D., and Atluri, S.N. (1998): A Local Boundary Integral Equation (LBIE) Method in Computational Mechanics, and a Meshless Discretization Approach, *Computational Mechanics*, Vol. 21, No. 3, pp. 223-235.